

# Electrochemical Behaviour of Industrial IrO<sub>2</sub>-Ta<sub>2</sub>O<sub>5</sub> Anodes for Copper Electrowinning

Wenting Xu<sup>1</sup>, Geir Martin Haarberg<sup>1</sup>, Svein Sunde<sup>1</sup>, Frode Seland<sup>1</sup>, Arne Petter Ratvik<sup>2</sup>, Erik Zimmerman<sup>3</sup>, Torjus Åkre<sup>4</sup>

<sup>1</sup>Department of Materials Science and Engineering, Norwegian University of Science and Technology, NO-7491 Trondheim, Norway

<sup>2</sup>SINTEF Materials and Chemistry, NO-7491 Trondheim, Norway

<sup>3</sup>Permascand AB, Folkets Husvägen 50, SE-84010 Ljungaverk SE, Sweden

<sup>4</sup>Glencore Nikkelverk AS, Vesterveien 31, NO-4013 Kristiansand S, Norway

In this work, industrial IrO<sub>2</sub>-Ta<sub>2</sub>O<sub>5</sub> anodes calcined at different temperatures were investigated. The results show that the calcination temperature has significant influence on the surface microstructure including the crystallinity and the preferred orientation of IrO<sub>2</sub> crystallite of the formed IrO<sub>2</sub>-Ta<sub>2</sub>O<sub>5</sub> binary oxide. The IrO<sub>2</sub> phase is partially amorphous at low calcination temperature in the present study. The (101) IrO<sub>2</sub> planes dominate at low or moderate calcination temperatures, whereas the (110) IrO<sub>2</sub> orientation was preferred at the highest calcination temperature. Surface morphology of the anodes was revealed as mud-cracks surrounded by a flat area with plenty of scattered nano-IrO<sub>2</sub> crystallites. The size of the nano-IrO<sub>2</sub> crystallites is calcination temperature dependent, which in turn determines the electrochemical active surface area (ECSA). In this IrO<sub>2</sub>-Ta<sub>2</sub>O<sub>5</sub> binary oxides coating, (101) IrO<sub>2</sub> was found to have higher catalytic activity than (110) IrO<sub>2</sub> with respect to the oxygen evolution reaction (OER). The moderate temperature is suggested as the best calcination temperature for this certain anode regarding the ECSA, electrocatalytic activity for OER and stability potential.

Keywords: IrO<sub>2</sub>-Ta<sub>2</sub>O<sub>5</sub>, microstructure, calcination temperature, catalytic activity, oxygen evolution reaction

## Introduction

The oxygen evolution reaction (OER), as the main anodic process in copper electrowinning (EW) in sulphate electrolytes, determines the anodic potential and the overpotential for this reaction which influences the total cell

potential [1]. Therefore, identifying an efficient anode catalyst to facilitate the OER by lowering the overpotential has been considered an important research field over many decades in copper EW [2, 3]. In addition, the stability and lifetime of the anodes have to be considered as well for industrial applications. With respect to the materials properties, IrO<sub>2</sub>-Ta<sub>2</sub>O<sub>5</sub> oxides mixture is suggested to be one of the best OER catalysts in industrial copper EW considering both catalytic activity and stability, and it is known as dimensionally stable anode (DSA). Titanium as substrate for supporting this catalyst will then be used.

The IrO<sub>2</sub>-Ta<sub>2</sub>O<sub>5</sub>/Ti anodes are usually prepared by thermal decomposition of a precursor containing iridium and tantalum salts. The pretreatment of the substrate and the thermal decomposition processes influence the properties of the anode as well as the final coating composition. Comninellis and Vercesi [4] reported that 70%IrO<sub>2</sub>-30%Ta<sub>2</sub>O<sub>5</sub>/Ti gives the best electrocatalyst for OER. Similar composition as 65% IrO<sub>2</sub> - 35 % Ta<sub>2</sub>O<sub>5</sub> has been reported by Krýsa and co-workers [5]. Besides, it has been demonstrated that the electrocatalytic properties of the anode significantly depended on the catalysts microstructure such as surface morphology and phase composition [5-8]. This was attributed to the 'true' surfaces of the coatings which is the electrochemically active surface area (ECSA). It is known that the prepared IrO<sub>2</sub>-Ta<sub>2</sub>O<sub>5</sub> commonly has heterogeneous 'mud-crack' morphology which is surrounded by a flat area with dispersed IrO<sub>2</sub> and IrO<sub>2</sub> aggregates. The boundaries of IrO<sub>2</sub> crystallites are modified by amorphous Ta<sub>2</sub>O<sub>5</sub>. Otagawa and co-workers [6] included that the fine IrO<sub>2</sub> particles (around 30-100nm) dominate in the electrocatalysis during OER while the other IrO<sub>2</sub> particles only show little influence, such as the larger IrO<sub>2</sub> aggregates and the IrO<sub>2</sub> particles embedded in the cracks. Our group [9] has reported that even smaller nano IrO<sub>2</sub> particles of 10 nm or less, which are uniformly dispersed on the flat area of the coating, have very good catalytic activity for OER, especially with the coating of 50% IrO<sub>2</sub>. Xu and Scantlebury [8] also concluded that the anodes with 50-70 % IrO<sub>2</sub> have not only the largest ECSA but also the highest electrochemical activity, but IrO<sub>2</sub> with 70% is still the best regarding the anode stability. For industrial application electrode stability and service life are important. It was demonstrated that the deactivation mechanisms of IrO<sub>2</sub>-Ta<sub>2</sub>O<sub>5</sub>/Ti anode are generally attributed to the consumption of the active component in the coating layer and/or the passivation of the substrate beneath the coating layer, which mainly depends on the coating microstructure [10]. In the coating layer, the IrO<sub>2</sub> can be stabilized by inert Ta<sub>2</sub>O<sub>5</sub> which also provides protection for the Ti substrate, even though the dissolution of Ir during OER has been found by many related works [10-13]. It was proposed that the deactivation process of the anode is as follows: (1) the dissolution of coated oxides are the dominating stage, i.e. IrO<sub>2</sub> loss from preferential orientations of (110) and (101), (2) dissolution and anodic oxidation of the Ti substrate which then lead to coating detachment and failure of the anode [11-12]. Based on basic thermodynamic considerations, metal oxide always become unstable under OER conditions irrespective of the pH value [13], which means the lifetime of an oxide anode under OER will always be limited. Therefore, either enhancing the stability of the coating layer to prolong the dissolution process or improve the electrocatalytic activity to make OER more efficient by modification of the coating microstructure are still hot topics in DSA research.

As mentioned above, the thermal decomposition condition is one parameter which significantly influences the microstructure and catalytic properties of the IrO<sub>2</sub>-Ta<sub>2</sub>O<sub>5</sub>/Ti anode. Many efforts have been carried out to illustrate this view and to find the optimum anode preparation procedure, such as the effect of calcination temperature,

solvent for precursors, coating thickness, ternary oxide mixtures or more, other coating techniques, and pretreatment of the titanium substrate [5, 14-17]. Most of the studies acknowledge the microstructure and electrochemical performance of the IrO<sub>2</sub>-Ta<sub>2</sub>O<sub>5</sub> anode with varying of the Ir : Ta ratio and calcination temperature in a wide range. The best Ir-Ta-O coating layer is recommended at a nominal IrO<sub>2</sub> content of 70% [4, 8, 14]. Even though, the intrinsic relationship between preparation conditions such as calcination temperature and catalytic properties of this type of anode is not fully understood.

In this contribution, a detailed study is carried out on industrial 70%IrO-30%Ta<sub>2</sub>O<sub>5</sub>/Ti anodes which were calcined at three different temperatures within a reasonable temperature range. Analytic investigation of the calcination temperature effect on microstructure has been illustrated based on the analysis of surface morphology, coating composition and crystallite orientation. It revealed that the OER catalytic activity is calcination temperature dependent. The relationship between the microstructure of the coating layer and the catalytic activity for OER was illustrated. A trend of calcination temperature dependence of preferable rutile IrO<sub>2</sub> orientation for this type anode has been demonstrated.

## Experimental

**Anode preparation.** – 70%IrO<sub>2</sub>-30%Ta<sub>2</sub>O<sub>5</sub> coated titanium samples were prepared by Permascand AB of Sweden. The titanium substrates were sand blasted and etched in oxalic acid before a thin house-made precursor films were applied to the Ti substrate by a brush coating technique. In order to evaporate the solvent in the precursors film, the coated titanium was dried at a fixed temperature<sup>1</sup> in the range of 400 - 550 °C in ambient air for about 10 - 20 minutes. The brushing and drying procedure was repeated for several times until the targeted loading of Ir amount was obtained. Finally, the coated titanium was calcined at the same temperature in ambient air for 1 hour. In this work, three different temperatures were applied for the calcination, denoted as ‘low T’, ‘moderate T’, and ‘high T’, respectively.

**Microstructure measurements.** – Surface morphology and chemical composition of the DSA samples were analysed using scanning electron microscopy (SEM, Zeiss Supra) combined with energy dispersive spectroscopy (EDS). X-ray diffraction (XRD) studies were carried out using Bruker AXS D8Advance with Cu K $\alpha$  radiation. Data were collected by varying the 2 $\theta$  angle from 10° to 80° with an increment of 0.02°. The crystalline structure and physical phase were calculated by the fitting of XRD patterns.

**Electrochemical studies.** – The electrochemical behaviour of the commercial anode samples was characterized by cyclic voltammetry (CV) and potentiodynamic polarization measurements to determine ECSA and electrocatalytic activity. The electrochemical experiments were carried out in a classical three electrodes system by using Gamry potentiostat, where Pt was counter electrode. A Teflon holder giving a 1 cm<sup>2</sup> electrode surface area was used. The electrode potential was measured against a reversible hydrogen electrode (RHE). All experiments were conducted at 60 °C with 0.9 M H<sub>2</sub>SO<sub>4</sub> aqueous solution as the electrolyte. Before each experiment run, the electrolyte was

---

<sup>1</sup> The exact calcination temperatures are confidential information, thereby cannot be provided.

de-aerated by purified argon gas for a few minutes. The CV measurements were recorded in a range between 0.15 V and 1.4 V vs. RHE with sweep rate varying between 5 - 500 mV/s. The scan rates for all polarization measurements were 5 mV/min in order to approach a static state during polarization. The IR drop during the testing was corrected for by measuring the electrolyte resistance using electrochemical impedance spectroscopy (EIS) at high frequency. The frequency range was from 0.1 Hz to 10 kHz with 10 points per decade, and the amplitude of the ac sine signal was 10 mV. Because the coating is porous and the gas evolution at the surface is very fast and will attack the coating, the active surface area would be changed [6]. Initialization of the anodes to be tested thereby is necessary before starting in-situ measurement, hence 200 CV cycles were run on all anode samples with sweep rate of 100 mV/s for all anode samples before recording a useful E-I curve. This initialization should be distinguished from the stabilization stage during realistic electrolysis. The former is to obtain a reproducible voltammogram on the tested coated surface of anode samples, whereas the latter is to achieve the stable surface situation for a constant overpotential for OER.

## Results and Discussion

The XRD data of the anode samples are shown in Fig.1, in which only IrO<sub>2</sub> rutile phase and Ti phase have been identified. Apparently the Ta<sub>2</sub>O<sub>5</sub> phase was amorphous for all samples. The crystallinity of the IrO<sub>2</sub> phase in the coating layer can be represented by the intensity of peaks related to IrO<sub>2</sub>. Obviously the crystallinity is improved by increasing the calcination temperature. Very broad IrO<sub>2</sub> peaks are observed in the coating which was calcined at low temperature. It means that the crystallization of this sample is very poor, and it could be amorphous. With high calcination temperature, the coating layer is not possible to be fully oxidized since the calcination temperature was less than 600°C according to Roginskaya's work [18]. Four crystallite orientations were observed among the IrO<sub>2</sub> related peaks, which are (110), (101), (211) and (200). The (211) facet of IrO<sub>2</sub> cannot be detected in the coating of 'low T' due to the low crystallinity. The texture coefficients ( $TC_{(hkl)}$ ) of IrO<sub>2</sub> were calculated by using Eq. 1 [19]. As can be seen in Fig.2, (110) is the preferred crystallite orientation at high calcination temperature. Similar results have also been found by Hu [20]. However, at low temperature we found (101) is preferred, which is different to Hu's results. This is a remarkable difference as industrial anodes are employed in our work. It should be mentioned that, according to the theory of texture coefficients, Eq. 1, only values of TC greater than one can be considered as having texture.

$$TC_{(hkl)} = \frac{I_{(hkl)} / I_{0(hkl)}}{\frac{1}{n} \sum_{i=1}^n I_{(hkl)} / I_{0(hkl)}} \quad [1]$$

where  $I_{(hkl)}$  is a measured intensity of  $(hkl)$  plane,  $I_{0(hkl)}$  is the standard intensity of the standard XRD patterns data, and  $n$  is the total number of reflections.

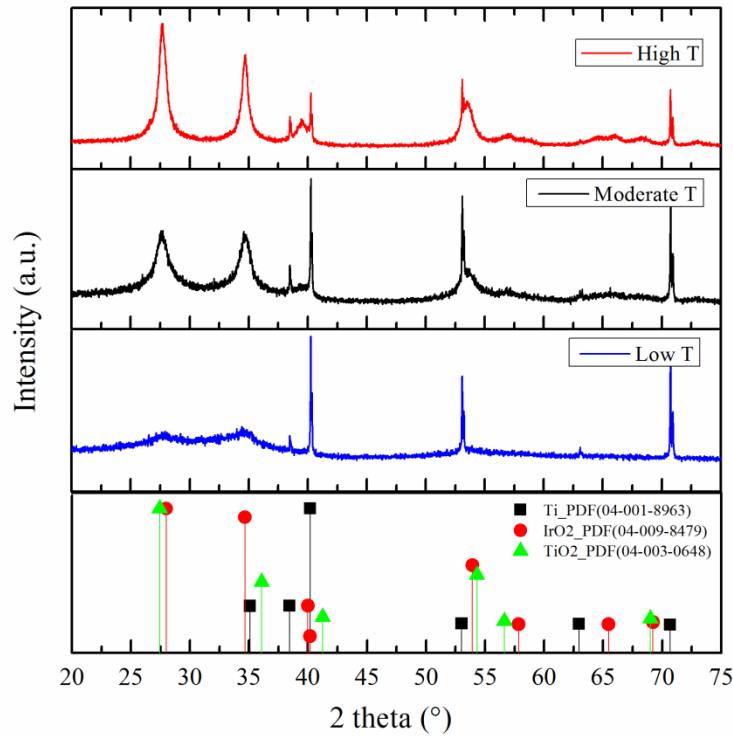


Fig.1. X-ray diffraction (XRD) patters for IrO<sub>2</sub>-Ta<sub>2</sub>O<sub>5</sub>/Ti anodes calcined at different temperature.

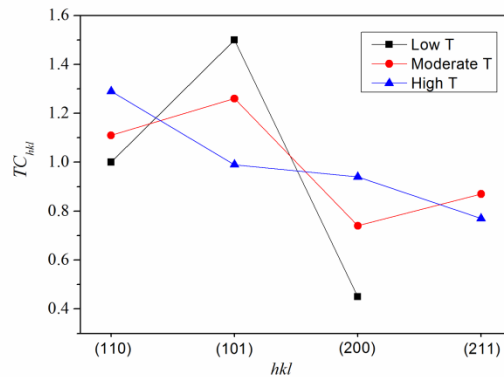


Fig.2. Texture coefficients of IrO<sub>2</sub> crystallites of all coatings regarding the XRD patterns.

The IrO<sub>2</sub> crystals grow during the thermal process. When the iridium chloride precursor has been decomposed the metal ions have been oxidized. The reactions related decomposition and oxidation are temperature dependent. At high applied temperature, the facilitated reaction can be obtained on both decomposition and oxidation processes [16]. Besides, all these chemical reactions take place on titanium substrate which would induce lattice strain into the formed coating layer, as well as the cooling down process after calcination. On the another hand, the presence of tantalum would form Ir(Ta)O<sub>2</sub> solid solution as a result of the interaction between Ir an Ta because of their

oxides both have rutile structure. As can be seen in Fig. 3, the d-spacing of most identified  $\text{IrO}_2$  crystalline planes become larger comparing with pure  $\text{IrO}_2$ . Interestingly, the d-spacing of (101) facets which calcined at relatively low temperature are slightly smaller. Combining this with temperature dependent preferable crystallite orientation, (101)  $\text{IrO}_2$  crystallites formed at either low or moderate temperature might be less stressed and/or less influenced by dissolved Ta atoms. It has been reported that (101) rutile  $\text{IrO}_2$  displays better catalytic activity since the length of the bond for Ir-O is shorter for (101) than the other facets [20]. It also has been reported that the stability of (101)  $\text{IrO}_2$  crystallites for OER is better than (110)  $\text{IrO}_2$  [11]. Thereby the low or moderate temperature could be considered as appropriate calcination temperature. Furthermore, another feature of the crystallization process is the influence of the size of the related crystals. The crystal size of  $\text{IrO}_2$  was roughly estimated based on full width at half maximum (FWHM) combined with using the Scherrer equation, as shown in Fig. 3(b). It indicates that the smallest grain size of (110)  $\text{IrO}_2$  crystal could be obtained when calcining the anode at moderated temperature. Even smaller (101)  $\text{IrO}_2$  grains could be obtained at low calcination temperature. Regarding the crystallinity of  $\text{IrO}_2$ , the grain sizes all grow bigger when calcined at comparably higher temperature.

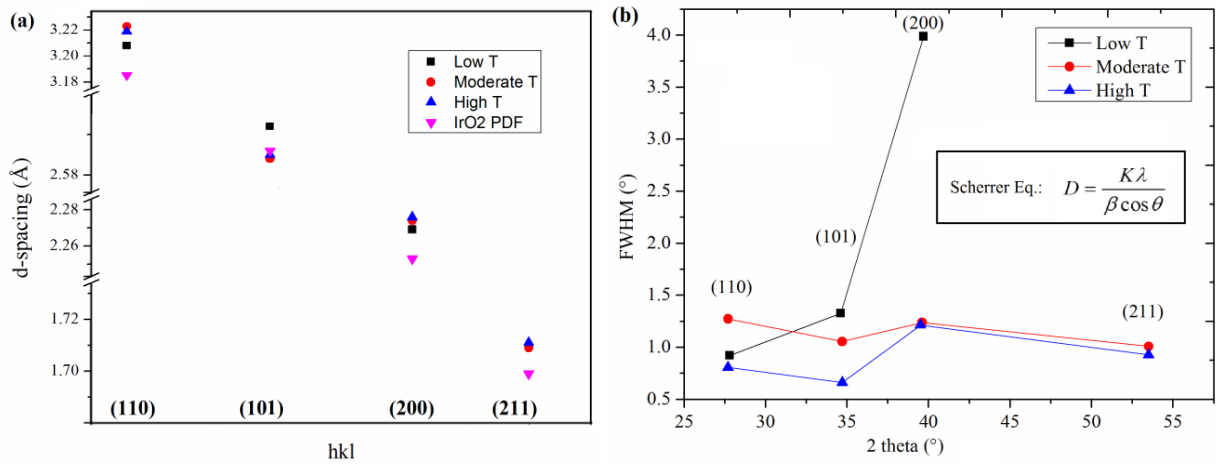


Fig.3. XRD fitting results (a) compared d-spacing values between all detected  $\text{IrO}_2$  crystallites and pure  $\text{IrO}_2$  crystalline, (b) full width at half maximum of all detected  $\text{IrO}_2$  planes, (insert is the Scherrer equation.).

Figure 4 shows the surface morphologies of  $\text{IrO}_2\text{-Ta}_2\text{O}_5$  coatings calcined at different calcination temperatures. All coating displays cracks on the surface, which are surrounded by a so-called 'flat area'. Those cracks are more or less similar, but they present different inside morphology. Many nano-scale particles have grown inside cracks during sintering. EDX analysis shows that the regions with particles are iridium enriched. Apparently these nano-particles are  $\text{IrO}_2$  crystals, which have formed during calcination and grow larger at higher calcination temperature. Besides, a few  $\text{IrO}_2$  nano particles have been observed within the 'flat area' outside cracks, but barely observed on the sample calcined at low temperature (in Fig.5). Ball-shape nano particles can be seen on the coating surface at moderate temperature, whereas nano cylinders as aggregates are generated at high temperature. Since the coating

calcined at the low temperature is partially amorphous, almost no nano  $\text{IrO}_2$  crystals formed on the flat area.  $\text{IrO}_2$  formation is a crystallization process preceded by nucleation during thermal decomposition, which always takes place in a site having a higher Gibbs energy. Hence, the crystallization may be heterogeneous and cause the surface to form with different morphological constituent. This is consistent with XRD analysis. It can cause both (110) and (101)  $\text{IrO}_2$  nanocrystallites to form in the 'flat area' which will grow larger at higher temperature, while (101) seem to be the preferred orientation at lower temperature. Apparently, the  $\text{IrO}_2$  aggregates are a result of (110) crystallites, where the (101) crystallites are formed as ball-shaped finer nanoparticles. It should be noticed that it is hard to distinguish the size difference between 'low T' and 'moderate T' in the inside cracks area of the nano  $\text{IrO}_2$  particles. This indicates that the nano- $\text{IrO}_2$  particles inside cracks could be mainly (101)  $\text{IrO}_2$  crystallites.

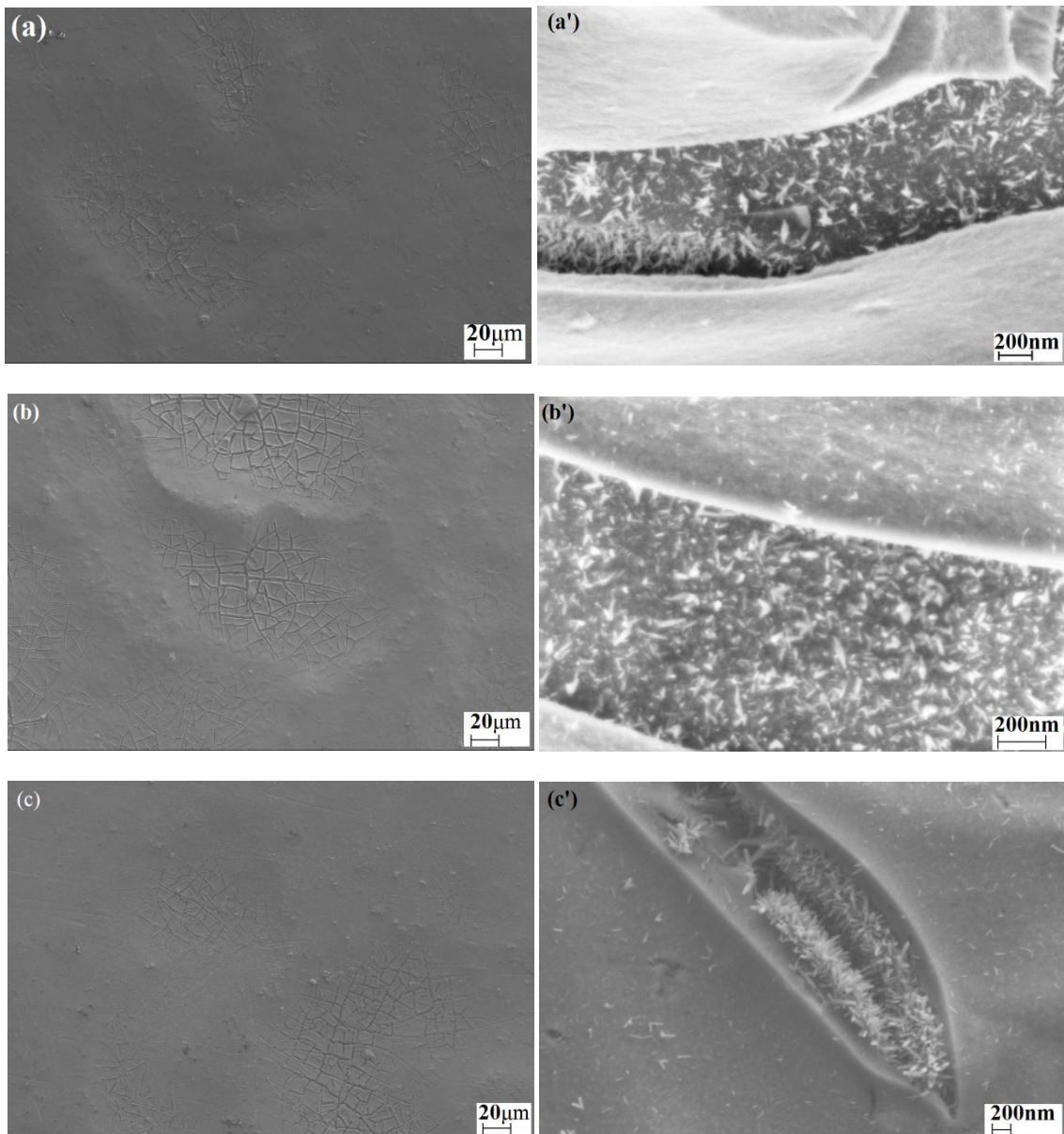


Fig.4. SEM images of IrO<sub>2</sub>-Ta<sub>2</sub>O<sub>5</sub>/Ti anode a&a' calcined at low temperature, b&b' calcined at moderate temperature, c&c' calcined at high temperature.

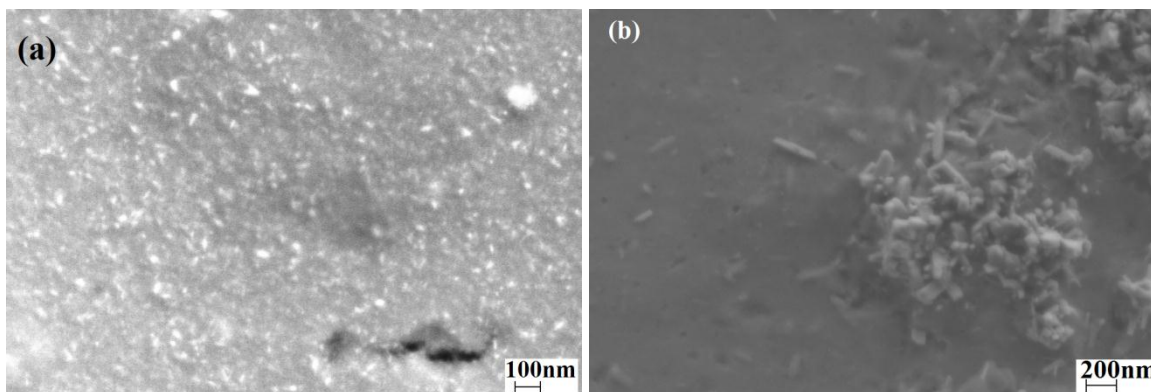


Fig.5. SEM images of the 'flat area' of the calcined anodes, (a) calcined at moderate temperature, (b) calcined at high temperature.

An interesting phenomenon has been found in our work as shown in Fig.6. The nominal content of iridium component in the coating layer is reduced by increasing calcination temperature even though the ratio of Ir : Ta of the coating is still 7:3 approximately. This should not be neglected because a slight difference may influence the coating properties; however, this is not yet concluded. Also, the nominal content of chlorine is reduced with increased temperature, which is evidence that the precursors were not completely decomposed at low temperature. However the amount of iridium chloride salt is small little to be detected by XRD.

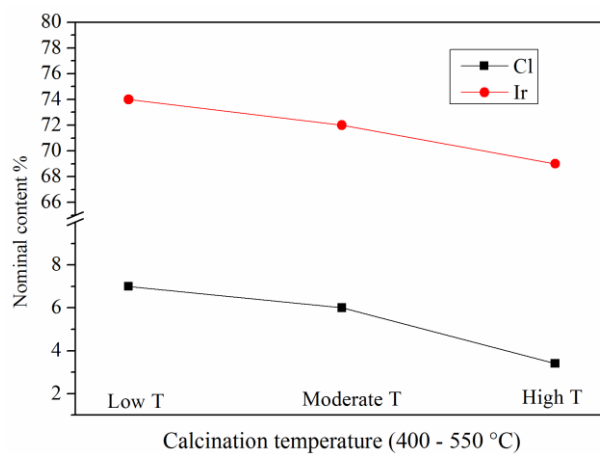


Fig.6. Ir:Ta ratio and residual chlorine content within the coating layer calcined at different temperatures.

The voltammetric behaviour observed for the calcined anodes are typical thermally prepared oxide coating, as shown in Fig.7a. The displayed broad peaks between the OER and the hydrogen evolution correspond to oxidation state transitions of noble metals (Ir<sup>3+</sup>/Ir<sup>4+</sup> in this case) [21]. It is clear that the peak current decreases with increasing calcination temperature and moves the onset potential of OER towards to higher potentials. Since the oxide compositions are almost equal, that change may be attributed to the surface morphology. The ECSA of those anodes are estimated by extrapolating the voltammetry charge  $q^*$ , which was obtained by integration of the CV curves thus measures the amount of protons exchanged with the electrolyte. According to the literature [4], the total charge  $q^*$  can be split into an inner and an outer charge, according to Eq. 2.

$$q^* = q_{\text{inner}} + q_{\text{outer}} \quad [2]$$

where the  $q_{\text{inner}}$  and  $q_{\text{outer}}$  are the charges related to the ‘inner’ and the ‘outer’ surface, respectively. The inner surface is the less accessible parts of the surface such as pores, cracks and grain boundaries, whereas the outer surface relates to the more accessible parts of the surface to the electrolyte. They also offer an approach to obtain the charge values by extrapolation both at  $v=0(q^*)$  and at  $v=\infty(q_{\text{outer}})$ .

As shown in Fig.7(b), the maximum value of all charges is obtained with the coating calcined at low temperature. With increasing calcination temperature, the maximum values of the charges decrease. This indicates that the ECSA would be decreased with increasing the calcination temperature of the anode. It implies the active sites would be decreased while calcining the coating at higher temperature. ECSA of the coating calcined at ‘low T’ is about 2 times larger than that at ‘moderate T’ and 5 times larger than the one at ‘high T’. Obviously ECSA is significantly affected by surface morphology. As we known, the inner charge is mainly determined by the inside of the coating, whereas the outer charge is mainly determined by the porosity of the surface and combined with the SEM analysis, it is concluded that:

- (1) Active sites of the anode surface are determined by the fine IrO<sub>2</sub> crystal, the more and finer, the more active sites contribute.
- (2) Amorphous IrO<sub>2</sub> has even more active sites on the surface due to the amorphous oxide is better dispersed throughout the coating.

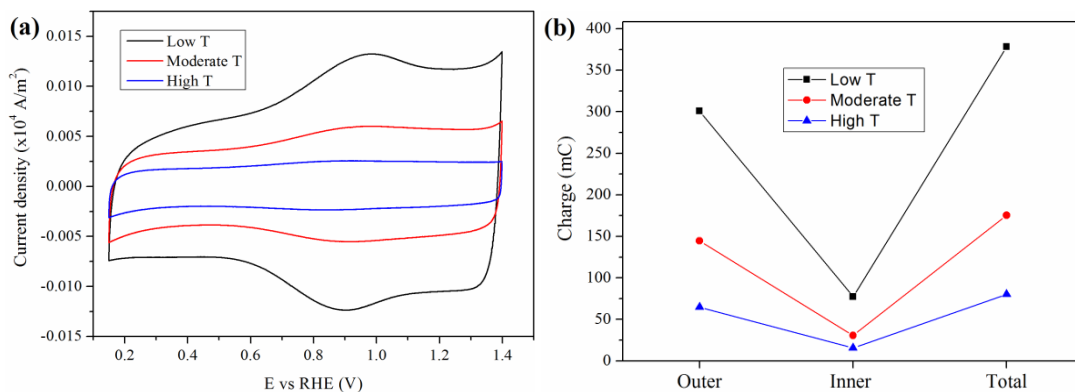


Fig.7. (a) Cyclic voltammetry of calcined anodes at different temperature, (b) Voltammetric charge calculated by integration and extrapolating of varying CV curves.

The IR-corrected polarization curves obtained for all calcined anodes are shown in Fig.8. As expected an increasing activity for OER is found as function of calcination temperature. Coating of ‘low T’ shows the best activity as a result of the biggest ECSA. In comparison the ‘high T’ is the worst. A relationship between current density and ECSA has been found occasionally. As an example, while at potential of 1.45V vs RHE, the passed current density for ‘low T’ is about 4 times than that for ‘moderate T’ and 25 times than that for ‘high T’. As shown previously, the ECSA value of ‘low T’ is about 2 times that of ‘moderate T’ and 5 times that of ‘high T’. It seems that the interrelationship of current density is the square of the interrelationship of ECSA for the examined anodes. Apparently the activity is determined by the amount of active sites. However, regarding Otagawa’s work [6], there is not enough evidence to say that the  $\text{IrO}_2$  aggregates and the nano  $\text{IrO}_2$  inside cracks are not productive active sites. We propose that all  $\text{IrO}_2$  phase would produce active sites.

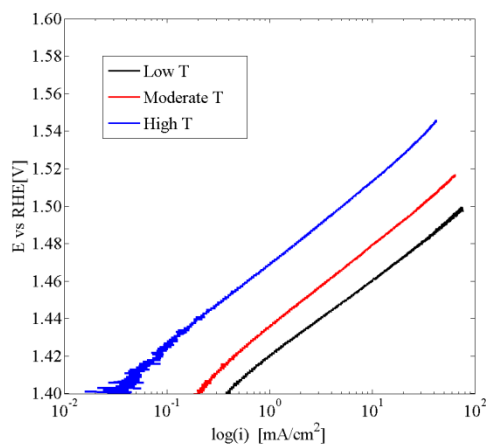


Fig.8. IR compensated polarization curves of different anodes, scan rate 5 mV/min.

In order to eliminate the surface roughness effects, the polarization curves have been normalized by respect to the outer charge, as shown in Fig.8. Here we can see the activity of ‘low T’ is still the best. The catalytic activity of ‘moderate T’ is just slightly lower than that of ‘low T’. It means the catalytic activity in unit active sites between these two samples is almost equivalent. The slight difference is believed to be due to the more amorphous anode calcined at low temperature. Amorphous IrO<sub>2</sub> has higher activity than crystalline IrO<sub>2</sub> which has been concluded by Thanawala et al. [23]. Therefore partial amount of amorphous IrO<sub>2</sub> in IrO<sub>2</sub>-Ta<sub>2</sub>O<sub>5</sub> mixture could increase the catalytic activity for OER. This demonstrates that the nano IrO<sub>2</sub> nested in the cracks most likely contribute to the activity. Because if only amorphous IrO<sub>2</sub> is regarded as active site, then this difference should be even larger. Additionally, regarding the preferred orientation of IrO<sub>2</sub> crystallites, (101) IrO<sub>2</sub> in IrO<sub>2</sub>-Ta<sub>2</sub>O<sub>5</sub> binary oxides have higher catalytic activity for OER. This also explains why the anode calcined at high temperature obtained the lowest catalytic activity on unit active sites.

Furthermore, Tafel slopes of all anodes within operational potential range seem quite similar, which is due to that the coatings are chemically equal. The slight difference is because of the amorphous phase of the coating which was calcined at low temperature. This implies that the OER mechanism may be different on the amorphous IrO<sub>2</sub> compared to the IrO<sub>2</sub> crystal phase. It has been reported in the case of amorphous RuO<sub>2</sub> that the rate determining step in OER for the amorphous phase was the combination of the adjacent Ru-OH groups, whereas on crystalline RuO<sub>2</sub> it was the dissociation of O-H bond in Ru-OH group [24]. A similar influence of amorphous IrO<sub>2</sub> in IrO<sub>2</sub>-Ta<sub>2</sub>O<sub>5</sub> on OER during electrolysis may be suggested, and further work should be done to verify this view. Besides, it seems that the lattice strain may have no influence on the catalytic activity. However, it is difficult to figure this out at present, and likewise for the influence of the solid solubility of Ir(Ta)O<sub>2</sub>. This will be considered in our future work.

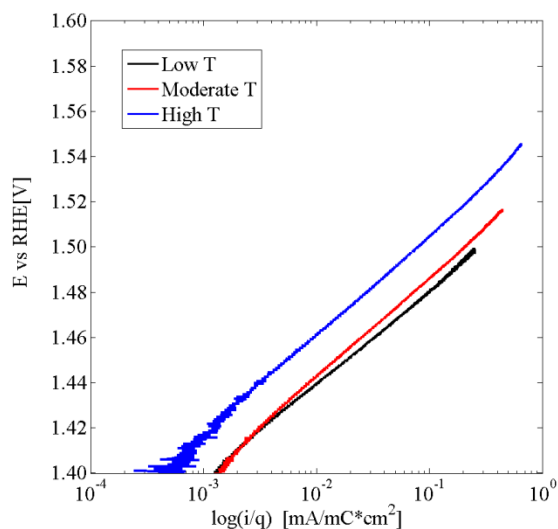


Fig.9. Normalized polarization curves on anodes calcined at difference temperature with respect to outer charge, which gives a measure for the electrocatalytic activity per unit active surface area

In addition, it has been reported that the (101) plane is far more resistant to corrosion than the other planes of IrO<sub>2</sub> since this plane is one of the most close-packed planes of the IrO<sub>2</sub> rutile phase [25]. Regarding this and the catalytic activity, the moderate temperature is considered as a proper calcination temperature for this type of IrO<sub>2</sub>-Ta<sub>2</sub>O<sub>5</sub> anode.

### Conclusion

The dependence of calcination temperature for DSA with commercial 70%IrO<sub>2</sub>-30%Ta<sub>2</sub>O<sub>5</sub> coating was investigated. Three different calcination temperatures were applied in terms of low, moderate and high temperature. The oxide coatings show critical mud-cracks surrounded by 'flat area' as main feature of surface morphology. Nano IrO<sub>2</sub> crystalline structure was formed both within inside cracks and on 'flat area' in all coatings after calcination. The grain size of IrO<sub>2</sub> is calcination temperature dependent, which increased by increasing calcination temperature. As a result the nano IrO<sub>2</sub> particles formed in the 'flat area' formed-aggregates when calcined at high temperature. At low calcination temperature, the coating was not fully decomposed. Almost no nano IrO<sub>2</sub> particles are generated on that 'flat area' since the 'flat area' dominated by amorphous coating. The IrO<sub>2</sub> crystals contribute and dominate the amount of active sites, which represents the ECSA. IrO<sub>2</sub> amorphous has more active sites than the IrO<sub>2</sub> crystalline structure. Additionally, the coatings calcined at low or moderate temperature show preferred (101) planes of IrO<sub>2</sub> crystallites, whereas the one calcined at high temperature is mostly (110) orientation preferred. It indicates that the nano-IrO<sub>2</sub> crystals as IrO<sub>2</sub> aggregates are a result of (110) crystallites, whereas the (101) crystallites are formed as ball-shaped finer nanoparticles. Except the ECSA, preferred orientation of IrO<sub>2</sub> also has influence on the catalytic activity for OER. Therefore the coating calcined at low temperature has the best catalytic activity for OER, whereas the one calcined at moderate temperature was almost similar. Regarding the lifetime of the anode, the moderate temperature is considered as the best calcination temperature in this specific case.

### References

- [1] W.C. Cooper, *J. Appl. Electrochem.*, **15**, 789 (1985).
- [2] G. Eggett and D. Naden, *Hydrometallurgy*, **1**, 123 (1975).
- [3] S. Trasatti, *Electrochim. Acta*, **45**, 2377 (2000).
- [4] C. Comminellis and G.P. Vercesi, *J. Appl. Electrochem.*, **21**, 335 (1991).
- [5] J. Krýsa, L. Kule, Mráz, I. Roušar, *J. Appl. Electrochem.*, **26**, 999 (1996).
- [6] R. Otagawa, M. Morimitsu and M. Matsunaga, *Electrochim. Acta*, **44**, 1509 (1998).
- [7] J.M. Hu, J.Q. Zhang, H.M. Meng, S.N. Cao, *J. Mater. Sci.*, **38**, 705 (2003).

- [8] L.K. Xu and J.D. Scantlebury, *J. Electrochem. Soci.*, **150**, B254 (2003).
- [9] K. Kawaguchi, G.M. Haarberg, M. Morimitsu, *ECS Trans.*, **16**, 41 (2009).
- [10] G.N. Martelli, R. Ornelas, G. Faita, *Electrochim. Acta.*, **39**, 1551 (1994).
- [11] J.M. Hu, H.M. Meng, J.Q. Zhang, S.N. Cao, *Corro. Sci.*, **44**, 1655 (2002).
- [12] L.K. Xu and J.D. Scantlebury, *Corro. Sci.*, **45**, 2729(2003).
- [13] T. Binninger, R. Mohamed, K. Waltar, E. Fabbri, P. Levecque, R. Kötz, T.J. Schmidt, *Scientific reports*, **5**, 12167 (2015).
- [14] G.P. Vercesi, J.Y. Salamin, CH. Comninellis, *Electrochim. Acta*, **36**, 991 (1991).
- [15] C.P. De Pauli and S. Trasatti, *J. Electroanalytical Chem.*, **145**, 538 (2002).
- [16] J.M. Hu, J.Q. Zhang, C.N. Cao, *Electrochim. Acta*, **403**, 257 (2003) .
- [17] L. Xu, Y. Xin, J. Wang, *Electrochim. Acta*, **54**, 1820 (2009).
- [18] Y.E. Roginskaya and O.V. Morozova, *Electrochim. Acta*, **40**, 817 (1995).
- [19] J.M. Hu, H.M. Meng, J.Q. Zhang, J.X.Wu, D.J. Yang, C.N. Cao, *J. Mater. Sci. Lett.*, **20**, 1353 (2001).
- [20] G.R.P. Malpass, A.J. Motheo, *J. Braz. Chem. Soc.*, **14**, 645 (2003).
- [21] S. Ardizzone, G. Fregonara, S. Trasatti, *Electrochim. Acta*, **35**, 263 (1990).
- [22] S.S. Thanawala, R.J. Baird, D.G. Georgiev, G.W. Auner, *Appl. Sur. Sci.*, **254**, 5164 (2008).
- [23] E. Tsuji, A. Imanishi, K. Fukui, Y. Nakato, *Electrochim. Acta*, **56**, 2009 (2011).
- [24] Z. Yan, Y. Zhao, Z. Zhang, G. Li, H. Li, J. Wang, Z. Feng, M. Tang, X. Yuan, R. Zhang, Y. Du, *Electrochim. Acta*, **157**, 345 (2015) .